Three-Dimensional Treatment of Convective Flow in the Earth's Mantle

John R. Baumgardner[1]

A three-dimensional finite-element method is used to investigate thermal convection in the earth's mantle. The equations of motion are solved implicitly by means of a fast multigrid technique. The computational mesh for the spherical problem is derived from the regular icosahedron. The calculations described use a mesh with 43,554 nodes and 81,920 elements and were run on a Cray X. The earth's mantly is modeled as a thick spherical shell with isothermal, free-slip boundaries. The infinite Prandtl number problem is formulated in terms of pressure, density, absolute temperature, and velocity and assumes an isotropic Newtonian rheology. Solutions are obtained for Rayleigh numbers up to approximately 10^6 for a variety of modes of heating. Cases initialized with a temperature distribution with warmer temperatures beneath spreading ridges and cooler temperatures beneath present subduction zones yield whole-mantle convection solutions with surface velocities that correlate well with currently observed plate velocities.

KEY WORDS: Mantle convection; multigrid; finite element; three dimensional; icosahedral mesh.

1. INTRODUCTION

Although sea floor spreading and continental drift have been widely accepted for almost two decades, the processes responsible for the observed pattern of plate motion still are not well understood. The present consensus is that the movements of the tectonic plates are the surface expression of a global pattern of solid state thermal convection in the earth's silicate mantle—the region that occupies the outer 45% of the earth's radius and some 83% of this volume.

---

[1] Theoretical Division, Group T-3, University of California, Los Alamos National Laboratory, Los Alamos, New Mexico 87545.

Estimates for the mantle's viscosity and temperature structure together with experimental data on the thermal properties of silicate minerals yield Rayleigh numbers in excess of 10^4 times that required for the onset of convection.[1] Therefore, the mantle is almost certainly convecting in a vigorous fashion.

Much effort has been devoted to obtaining more accurate estimates with better spatial resolution of the mantle's physical properties. In general such estimates must be inferred from seismic, gravity, heat flow, and topographic measurements made at or near the earth's surface. Recently seismic techniques have provided the ability to reconstruct the mantle's three-dimensional density structure, although the resolution is still severely limited.[2,3]

A highly desirable component in this task of relating the plate motions to the dynamic processes in the mantle is the ability to simulate numerically the convective flow field.[4,5] Because the problem is nonlinear and, in general also time dependent, even an incompressible and constant material property treatment in three dimensions has been considered beyond the reach of present computers.[6] This paper summarizes an approach that allows such three-dimensional time-dependent calculations and presents results for Rayleigh numbers up to 1000 times the value at which convection begins.

2. MATHEMATICAL FORMULATION

The mantle convection problem is formulated in terms of conservation equations of linear momentum, mass, and energy inside a spherical shell with appropriate boundary conditions. Rotational effects are neglected since the Coriolis force is extremely small compared with the viscous forces and since the centrifugal force causes the ratio of major radius to minor radius of the earth to depart from unity by only one part in three hundred. The inertial forces similarly are quite small relative to the viscous forces, and they also are omitted from the equations of motion. A linear and isotropic constitutive law is assumed so that the mantle is treated as an infinite Prandtl number Newtonian fluid.

Under these assumptions, the following equations describe the local behavior:

$$0 = -\nabla p + \rho \mathbf{g} + \nabla \cdot \tau \tag{1}$$

$$\frac{\partial \rho}{\partial t} = -\nabla \cdot (\rho \mathbf{u}) \tag{2}$$

$$\frac{\partial T}{\partial t} = -\nabla \cdot (T\mathbf{u}) - (\gamma - 1)\, T\nabla \cdot \mathbf{u} + \frac{[\tau : \nabla \mathbf{u} + \nabla \cdot (k\nabla T) + H]}{\rho c_v} \tag{3}$$

where

$$\tau = \mu[\nabla\mathbf{u} + (\nabla\mathbf{u})^T - 2I(\nabla \cdot \mathbf{u})/3] \tag{4}$$

and

$$p = p(\rho, T) \tag{5}$$

Here p denotes pressure, ρ density, $\mathbf{g}$ gravitational acceleration, τ deviatoric stress, $\mathbf{u}$ fluid velocity, T absolute temperature, γ the Grüneisen ratio, k thermal conductivity, H volumetric radiogenic heat production, c_v specific heat at constant volume, and μ dynamic viscosity. Equation (1) describes the balance among pressure gradient, buoyancy, and viscous forces. Equation (2) expresses the conservation of mass. Equation (3) describes the conservation of energy in terms of the absolute temperature. Equation (4) is the constitutive law, and (5) represents the equation of state as a suitable function of density and temperature. This compressible formulation that uses the primitive variables, p, ρ, T, and $\mathbf{u}$ is notably more general than the incompressible Boussinesq formulation commonly employed for such problems.

From seismic observations, the earth's outer core is known to be in the liquid state. Free-slip, isothermal boundary conditions are therefore appropriate for the inner boundary. Similar boundary conditions are also reasonable for the outer surface. For simplicity, the boundaries are also assumed undeformable.

A common measure of the vigor of the convection is the Rayleigh number R. For a plane layer of thickness d heated from below, the Rayleigh number is defined as

$$R = \frac{\alpha g \rho^2 \varDelta T d^3}{\mu k} \tag{6}$$

where α is the volume coefficient of thermal expansion, $\varDelta T$ is the temperature difference across the layer, and the other quantities are as defined above. When the layer is heated entirely from within, $\varDelta T$ is replaced by Hd^2/k. These definitions for Rayleigh number will be applied to the spherical shell, where d represents the shell thickness. The Rayleigh number at which the layer becomes unstable to the onset of convection is known as the critical Rayleigh number. For a spherical shell with a ratio of inner to outer radius corresponding to that of the earth's mantle, the critical Rayleigh number is about 1000 when the heating is entirely from the inner boundary and about 1800 when the heating is entirely from sources interior to the shell.[5]

3. COMPUTATIONAL STRATEGY

An efficient method for numerical solution of the system of equations in the previous section will now be described.[7] Briefly, it is a Eulerian finite-element formulation that utilizes a fast multigrid elliptic solver for the equations of motion. A nested set of almost uniform discretizations of the sphere, constructed from the regular isosahedron (Fig. 1), provides the basis for the multigrid procedure.[8] The successively finer meshes shown in Fig. 1 are obtained by construction of great circle arcs between side mid-points of the spherical triangles. The refinement process can be repeated to yield almost uniform triangulations of the sphere of any desired resolution.

The three-dimensional mesh is realized (Fig. 2) by replicating the spherical mesh at various radial positions to yield elements having the form of triangular prisms with spherical ends. Spherical barycentric coordinates are defined on each of the spherical triangles. The finite-element basis functions are Cartesian products of piecewise linear functions (the spherical barycentric coordinates) in the tangential direction and piecewise linear functions in the radial direction.

The calculations described in the next section use, as the finest mesh, one with 16 subdivisions of the original icosahedral sides (Fig. 1e) and 16 layers of elements in the radial direction. Such a mesh has 43,554 nodes and 81,920 elements. The velocity field is discretized in terms of the piecewise linear basis functions identified with the nodes, while the density, temperature, and pressure fields are discretized using piecewise constant functions defined on the elements. Hence, there are 130,662 degrees of freedom associated with the velocity field and 81,920 degrees of freedom in the scalar density and temperature fields.

Because the basis functions are factorable into tangential and radial parts, the finite-element operators may be generated and stored inexpensively in factored form and assembled only as they are applied. The symmetries of the icosahedron are exploited to reduce further the costs of generation, storage, and assembly. Combining pairs of the original 20 icosahedral triangles to form ten diamonds on the sphere leads to a data structure composed of ten logical cubes. Such a structure is well suited to vector processing and multitasking. On a vector machine such as a Cray, this implementation yields a speed corresponding to one addition or multiplication, on the average, for every two computer-clock cycles for the code as a whole.

The key to the overall efficiency of the numerical approach is the multigrid solution of the equations of motion. The multigrid method requires only order n machine operations to solve an elliptic system of n equations. It is therefore competitive with spectral methods that utilize the FFT
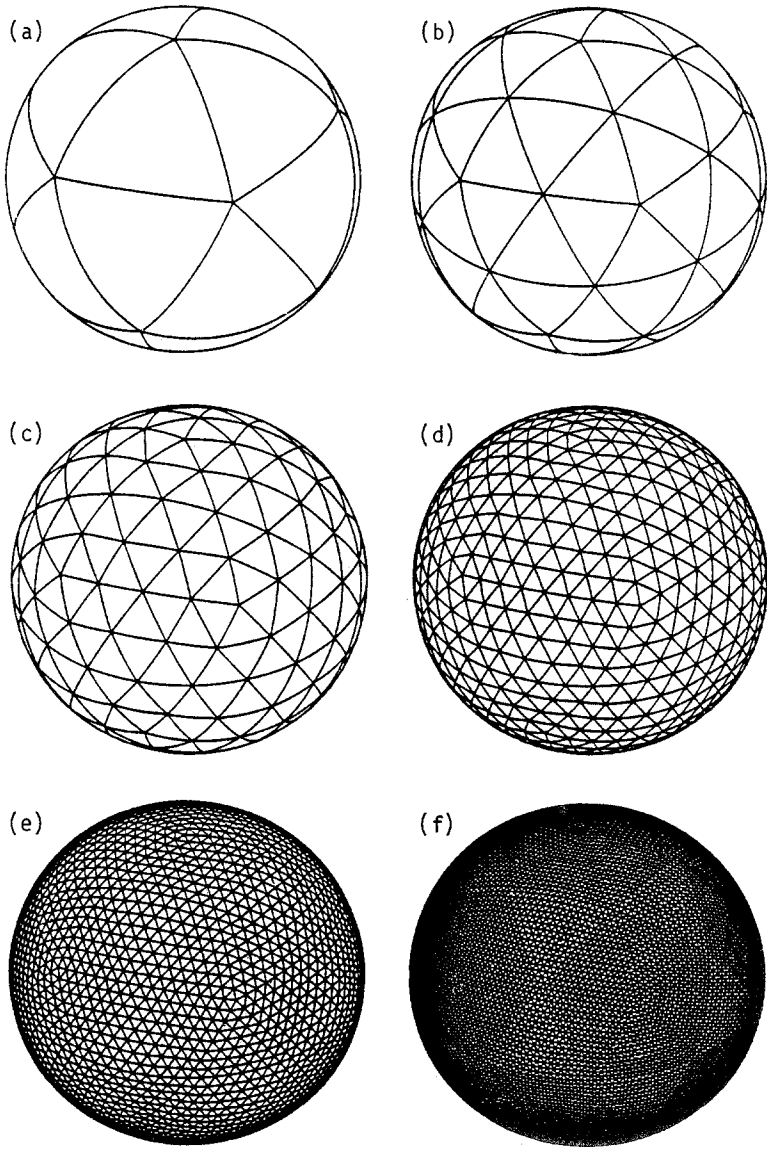
Fig. 1. (a) Mesh produced by projection of the regular icosahedron onto the sphere. (b)–(f) Successive mesh refinements obtained by connecting midpoints of triangle sides with great circle arcs.
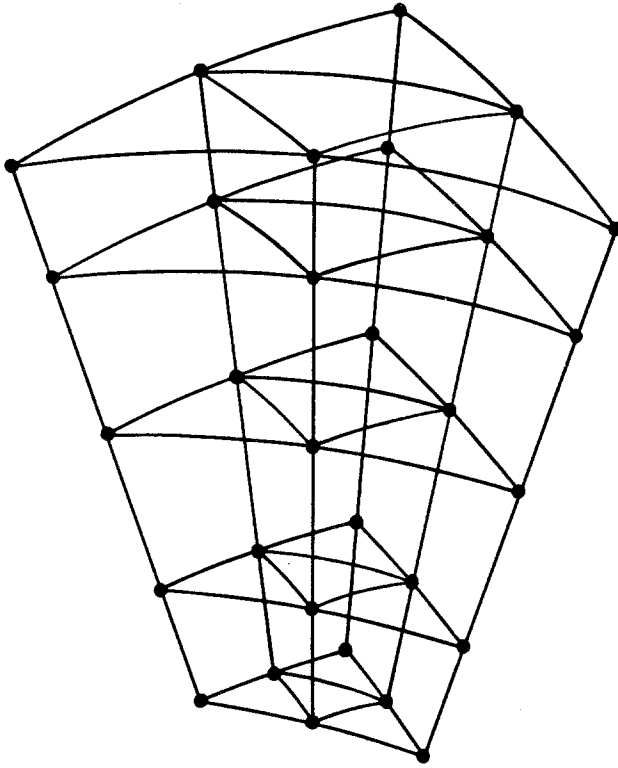
Fig. 2.   Portion of three-dimensional finite element mesh. Elements have three planar faces
and two faces that are spherical triangles.

algorithm and can be applied where harmonic representations are
inappropriate. As implemented for the presented application, the iterative
multigrid algorithm first projects the residual field from the finest grid into
all the coarser grids. Then beginning with the coarsest grid, it uses a local
approximate inverse at each grid level to improve the correction field as
this correction field is interpolated back to the finest grid. The local
approximate inverse operators are constrained to have the same graph,
that is, to involve the same nodes in the mesh, as the forward finite-element
operators. A least-squares procedure is used to generate the inverse
operators from the forward operators. The multigrid algorithm yields a
reduction in the norm of the residual of a factor, typically, of three to ten
per iteration. The cost per iteration is equal approximately to four
applications of the forward operator.

    A conservative cell-wall advection technique is used to treat the
$\nabla \cdot (\rho \mathbf{u})$, $\nabla \cdot (T\mathbf{u})$, and $\nabla \cdot \mathbf{u}$ terms in Eqs. (2) and (3). Heat conduction is
handled in a simple finite-difference fashion.

The strategy for solving the system (1)–(5) is first to compute the pressure field from the density and temperature fields via the equation of state, to solve (1) implicitly for the velocity field using the multigrid solver, to compute from (2) and (3) the rates of change of the density and temperature fields using this velocity field, and to take a time step and update the density and temperature fields. Actually, a second-order time integration scheme is used that requires two such solution passes per time step. For optimum performance, the time step is dynamically adjusted so as to require but one iteration of the multigrid algorithm to maintain a prespecified level of accuracy in the solution of the equations of motion.

For the case of constant viscosity and almost incompressible flow, the divergence of the stress in Eq. (1) reduces to the viscosity times the Laplacian operator applied to the velocity field. For this simplified treatment, the cost per time step for the mesh with 81,920 elements is approximately 2.0 CPU seconds on the Cray X. For high Rayleigh number problems where fine resolution is needed near the shell boundaries, typically 2000 time steps are required per convective overturn. Thus the cost for such calculations on the current generation of machines is still far from modest.

4. RESULTS

This section describes calculations from a Fortran-coded version of the numerical method just reviewed. In addition to the assumptions mentioned in Section 2, the calculations further assume constant material properties throughout the shell and almost incompressible flow. Although mantle viscosity is strongly temperature and pressure dependent and although there are mineral-phase changes through the upper mantle as well as some 30% compression across the lower mantle, the simplified model provides the ability to investigate the fundamental character of the three-dimensional convection in a spherical shell, whose average properties closely match those of the mantle.

The assumption of almost incompressible flow admits a simple equation of state

$$p = K[(\rho - \rho_0)/\rho_0 + \alpha(T - T_0)] \tag{7}$$

where K is the bulk modulus, ρ_0 the reference density, and T_0 the reference temperature. The radius ratio of the spherical shell used to represent the mantle is chosen to be ratio of the core–mantle boundary to the earth's outer radius, or 0.547. The model therefore assumes a whole-mantle style of convective flow.

The resolution of the mesh imposes a limit on the Rayleigh number because of zoning requirements for the boundary layers. This maximum Rayleigh number is of the order of 10^6, when heating is primarily from below. While the Rayleigh number estimated for the mantle is of the order of 10^7, this resolution nevertheless allows calculations far into the super-critical region—some 10^3 times the critical Rayleigh number compared with 10^4 for the earth.

Under the foregoing constraints, the problem needs be examined in terms of only three imputs—the Rayleigh number, the extent of internal heating, and the initial conditions. Briefly, the calculations reveal notable differences in the character of the convection in cases for which the heating is mostly from below compared with cases dominated by internal heating. When heating is mostly from below, i.e., from the inner boundary, tem-porally stable solutions are obtained up to the highest Rayleigh numbers investigated. At the higher Rayleigh numbers, the upwelling flow constricts to a small number of narrow plumes. The number of plumes is only weakly related to Rayleigh number. By contrast, mostly internal heating yields time-dependent solutions when the Rayleigh number exceeds about 150 times the critical value. In these solutions it is the downwelling flow that displays plumelike character. Furthermore, the number of plumes increases strongly with Rayleigh number. When heating is mostly from below, high spatial frequency components in the initial condition dissipate quickly, but the low-frequency components persist for many convective overturns. When heating is mostly internal, memory of the initial condition is brief, especially at the higher Rayleigh numbers.

Since the character of the motion observed at the earth's surface strongly resembles the low-frequency nature of convection when heating is mostly from below, it seems probable that this indeed is the convective style that prevails in the mantle. Before considering this issue further, some examples will be presented that illustrate the general trends.

Figure 3 shows the stable solution obtained for a case heated entirely from below at a Rayleigh number of 5×10^5, or approximately 500 times critical. This case used a $L = 3$, $M = 3$ sectorial harmonic as its initial tem-perature distribution. Figure 3 is plotted in Mercator projection so that the whole sphere, apart from small regions at the poles, can be displayed in a single frame. Color is used to represent the temperature field. Arrows denote tangential velocity, triangles radially upward velocity, and squares radially downward velocity. The three frames depict different radial positions in the spherical shell.

The solution in Fig. 3 consisting of three zones of upwelling flow represents the preferred pattern for spherical shells of radius ratio near 0.55 when heating is entirely from below for Rayleigh numbers just above
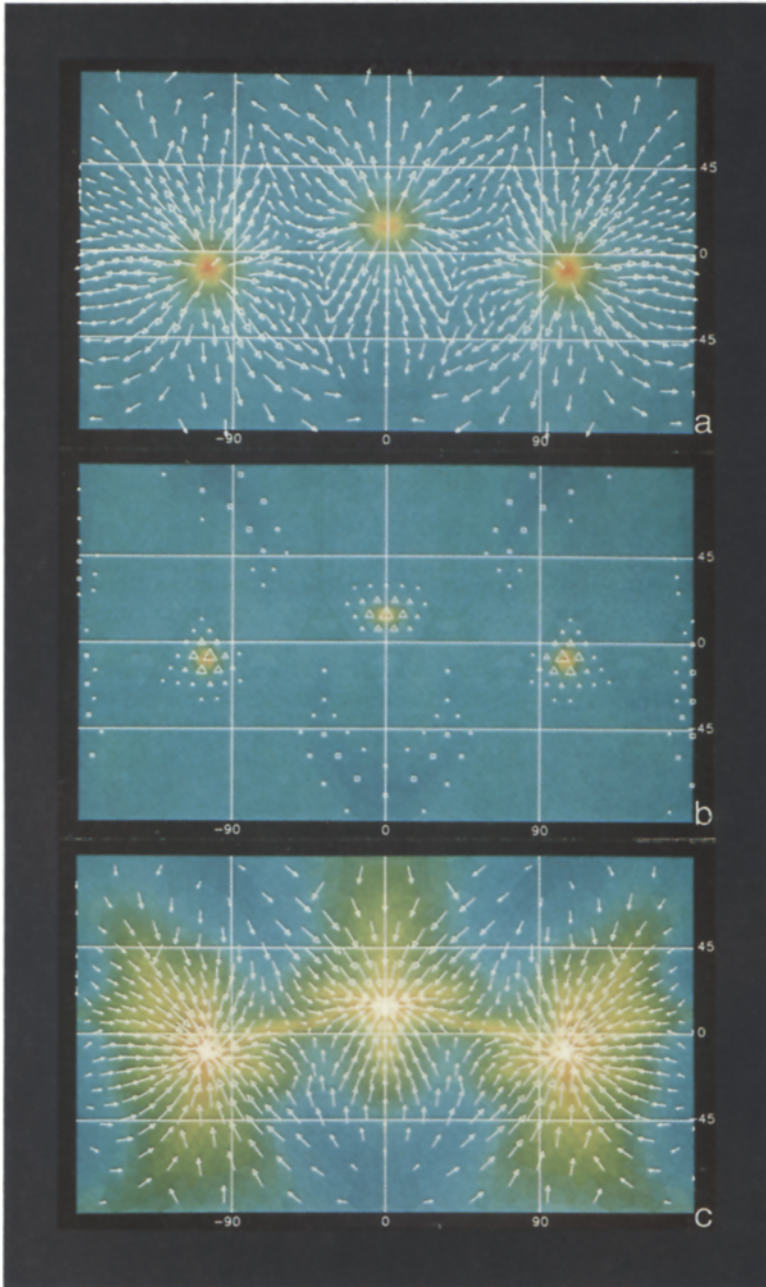
Fig. 3. Convection solution shown in Mercator projection for spherical shell heated only from below with Rayleigh number 5×10^5. Arrows represent tangential velocity in magnitude as well as in direction. Triangles denote radially outward velocity and squares radially inward velocity. Temperature is depicted by color. (a) Solution near outer boundary with temperature range between 320 and 1630 K. (b) Solution at middepth with temperature range between 660 and 2800 K. (c) Solution near inner boundary with temperature range between 2120 and 3750 K. Note the localized character of the upwelling flow. Solution is stable with time.
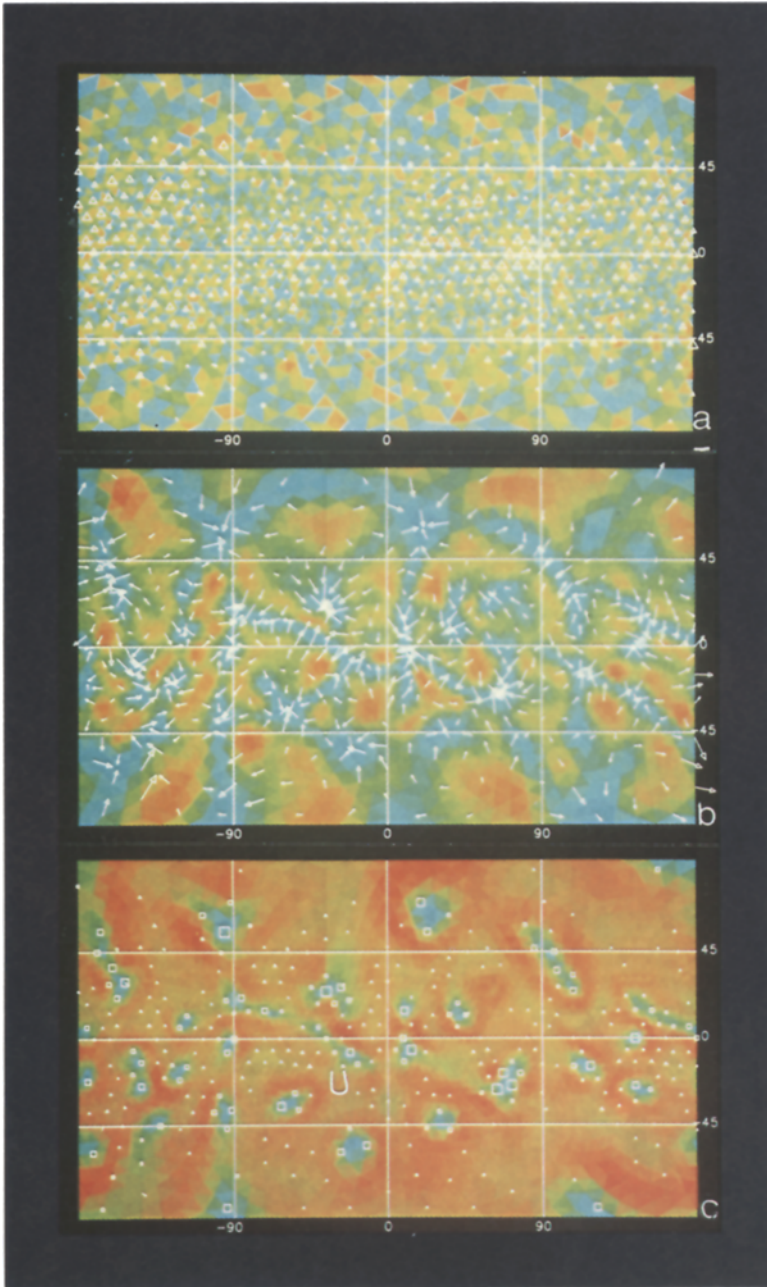
Fig. 4. (a) Example of random initial temperature distribution. (b), (c) Solution near the outer boundary and at middepth, respectively, for a case with purely internal heating and Rayleigh number of 5×10^6. Temperatures vary with depth approximately as in Fig. 3. Note the high spatial frequency character of the pattern. Solution is time dependent with the downwelling columns in (c) displaying a slow drift.
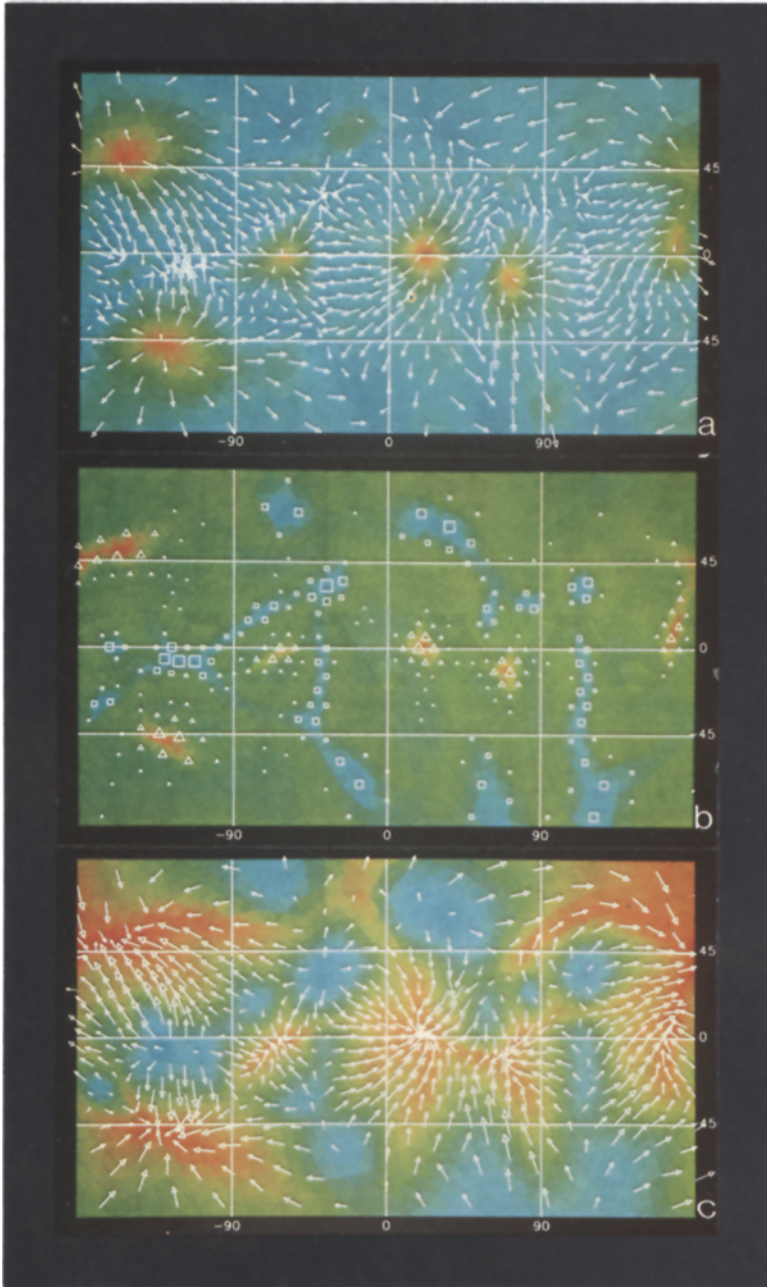
Fig. 5. Convection solution for spherical shell with 50% internal heating, 50% heating from below, Rayleigh number 5×10^5, and initialized with a random temperature distribution. Pattern consisting of six upwelling plumes is realized after approximately two convective overturns and changes very little during three additional overturns. Solution at this final time is shown (a) near the outer boundary, (b) at middepth, and (c) near the inner boundary. Apart from an increased number of upwelling zones, the solution is similar in character to that of Fig. 3 in which the heating is entirely from below.
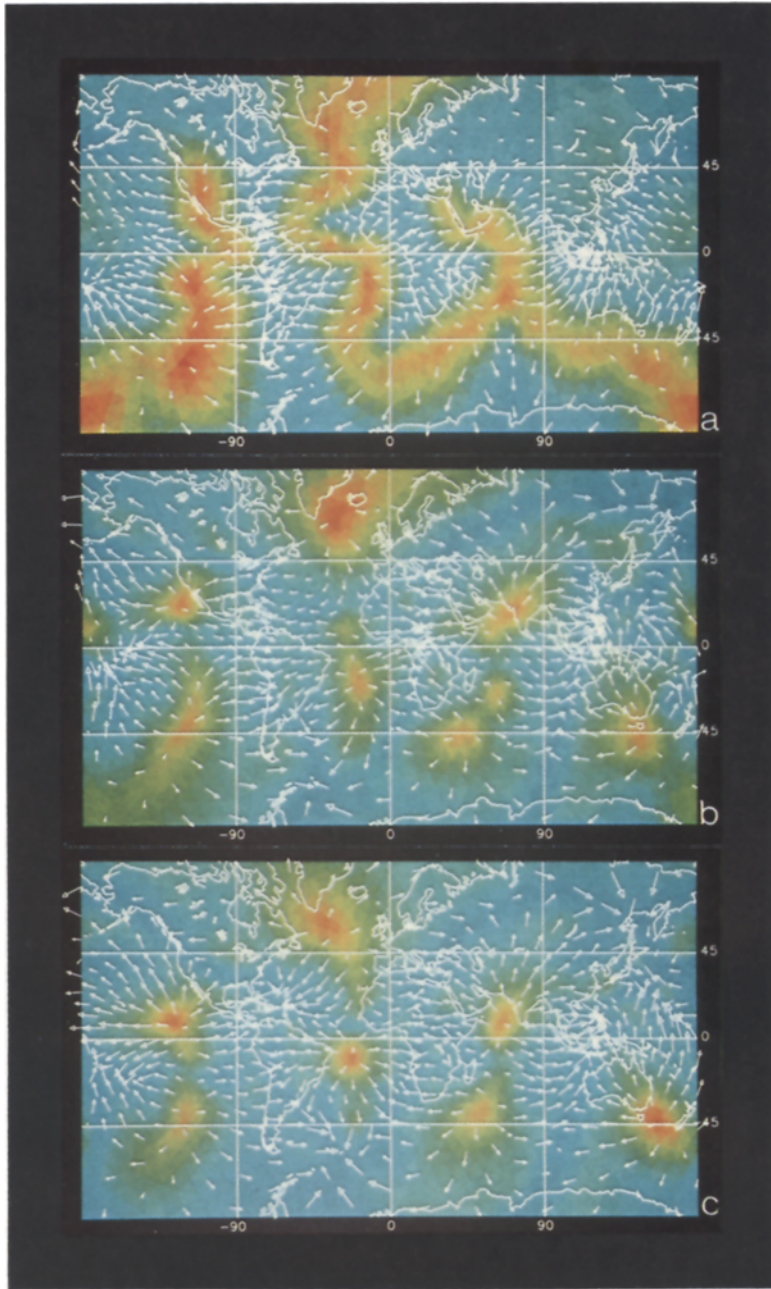
Fig. 6.   Time history for a case identical to that of Fig. 5 except for initial condition. Here the initial temperature distribution contains a positive anomaly beneath mid-ocean ridges and a negative anomaly beneath subduction zones on the earth. (a)–(d) are snapshots of the solution near the outer boundary at 0.1, 1.3, 2.6, and 3.9 convective overturns, respectively. (e) and (f) are at middepth and at the inner boundary at the last time of 3.9 overturns. (g) through (l) provide a somewhat better visualization of (d). Remarkable correlation exists between the surface velocities and plume locations in this solution with the plate velocities and sites of mid-ocean volcanic activity observed for the earth.
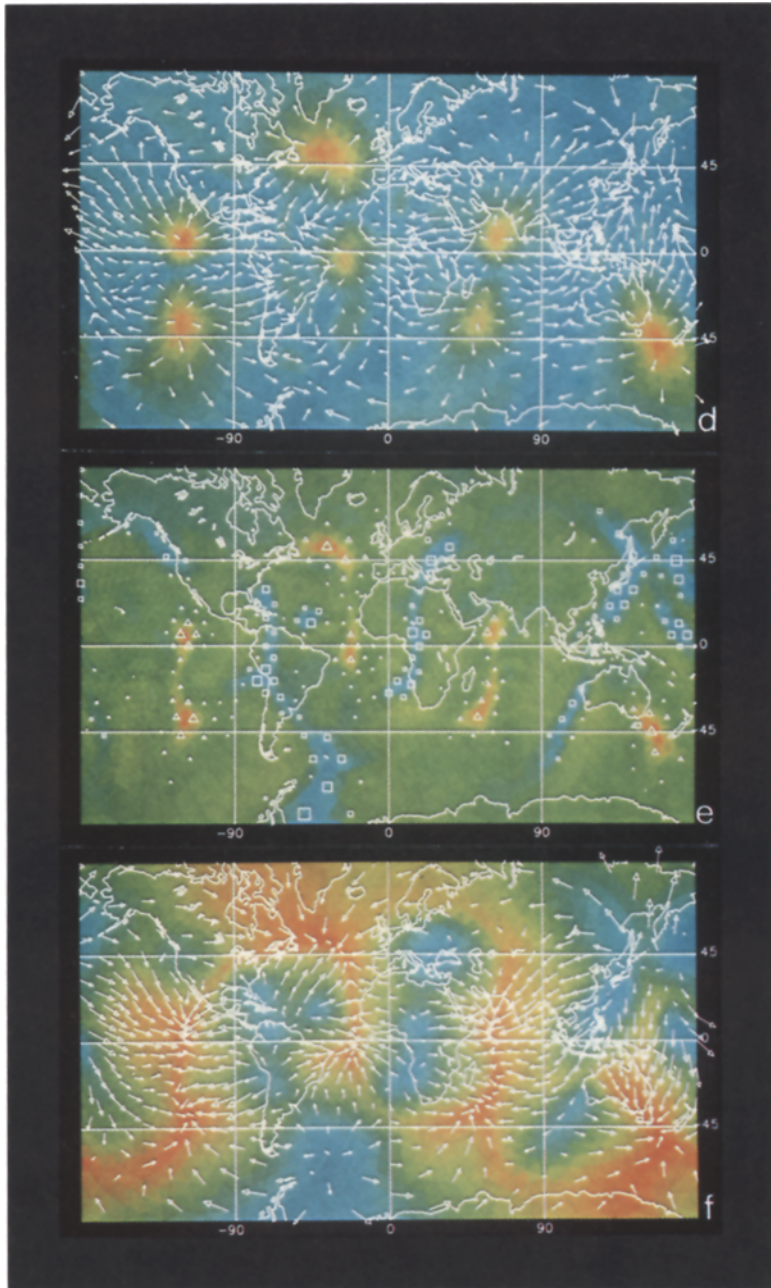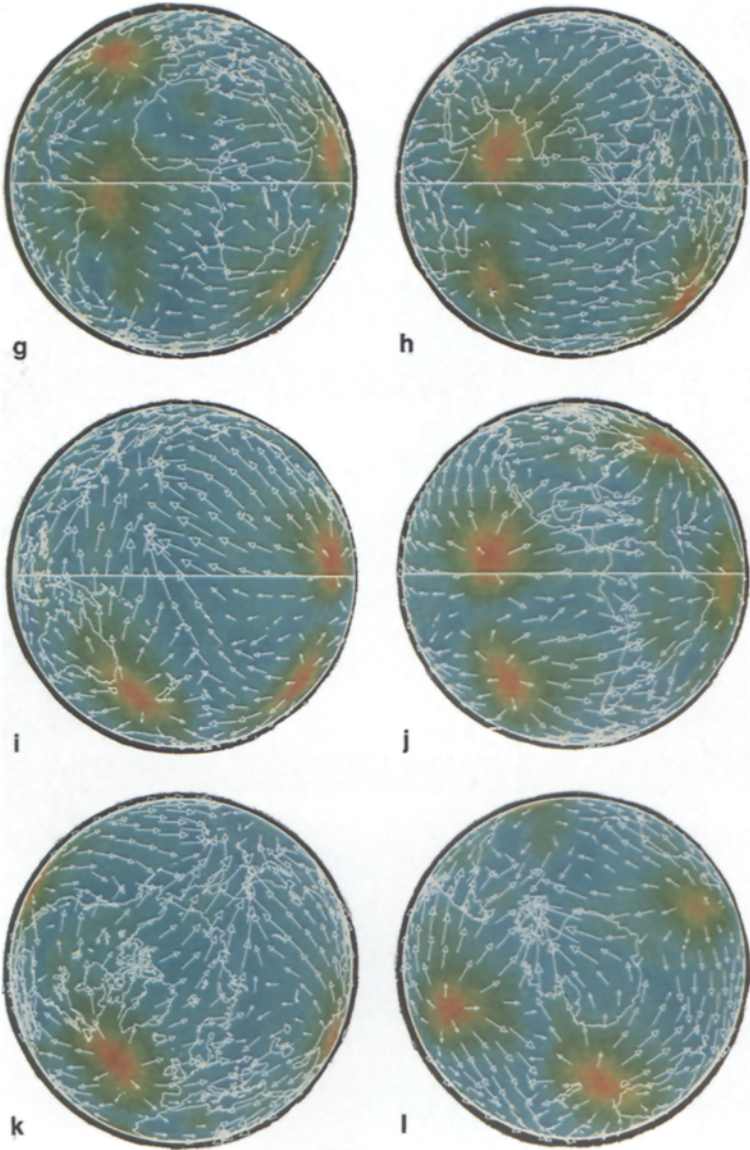
Fig. 6 *(continued)*

Fig. 6 *(continued)*

critical up to at least 10^6. It is approached in the steady state from almost all initial conditions. At Rayleigh numbers on the order of only a few times critical, the solution resembles an $L = 3$, $M = 3$ sectorial harmonic with a small added amount of the $L = 2$, $M = 2$ harmonic. The noteworthy aspect of this mode of heating is the small number of upwelling zones, a feature that persists to the highest Rayleigh numbers studied.

The middle and bottom frames of Fig. 4 show the solution for a case heated entirely from within, with a Rayleigh number of 5×10^6, or about 2800 times critical. The large number of downwelling plumes are evident. The top frame of Fig. 4 is the random initial condition used for this case. At this high Rayleigh number, the convection has the character of diffuse upwelling flow, with downwelling occurring in tight columns that drift with time but which are distributed more or less uniformly over the sphere. A notable aspect of this mode of heating is the high spatial frequency character of the convective flow at high Rayleigh number. The high-frequency pattern appears quickly regardless of the initial condition.

In the earth's mantle, there is both internal heating as a consequence of radioactive elements in the mantle rock and heat flowing into the mantle from the core. The relative contributions from these two sources are not well constrained by present observations. Motivation exists, therefore, to investigate convective behavior when there is a combination of internal heating and heating from below.

Figure 5 shows the solution obtained for a case random initial conditions, a Rayleigh number of 5×10^5, and 50% internal heating. There are five upwelling plumes with the suggestion of a sixth. The downgoing flow consists mostly of pieces of the cold outer boundary layer that descend in sheetlike fashion and maintain sheetlike character most of the way to the inner boundary. This shapshot was after approximately five convective overturns, and the solution appears to be stable in time.

Several observations can be distilled from calculations with a mixture of internal heating and heating from below. When the proportion of internal heating is less than 75%, the convective style has the essential character of heating purely from below with upwelling at cell centers. Almost steady flow is realized. At Rayleigh numbers (based on the heating-from-below formula) above 100 times critical, the flow is characterized by a small number of upwelling plumes. The number of plumes seems to be only weakly influenced by the amount of internal heating and to increase slowly with increasing Rayleigh number. Six plumes seem to be preferred for $R = 10^6$, and 50% internal heating.

The spatial frequencies and the character of the downwelling flow in Fig. 5 display similarities with observable tectonic features of the earth. The outer stiff portion of the earth known as the lithosphere, typically 50 to

100 km in thickness, is broken into seven major plates. The plates are moving apart at mid-ocean ridges and are being subducted into the mantle at ocean trenches. To explore the possibility of a correlation between the distribution of the ridges and trenches and a global pattern of convective flow in the mantle, cases were run with initial conditions that incorporate the current ridge/trench pattern. Specifically, the initial temperature distribution contained a positive perturbation beneath present ridges and a negative perturbation beneath subduction zones.

Figure 6a shows the solution near the beginning of a calculation using this special initial condition, a Rayleigh number of 5×10^5, and 50% internal heating. Except for the initial condition, this case is identical with that of Fig. 5. Figures 6b and 6c are snapshots of the solution near the outer boundary at approximately 1.3 and 2.6 convective overturns, respectively. Figures 6d–l represent a snapshot of the solution after approximately 3.9 convective overturns.

Among the noteworthy features of this solution is that the sheetlike pattern of upwelling associated with the initial temperature distribution quickly constricts into seven well-defined plumes which then persist for several convective overturns. The locations of these plumes correlate surprisingly well with volcanic activity in Iceland, the Horn of Africa, the Kerguelen Islands, and Hawaii. The surface velocities likewise agree well in direction and relative magnitude with observed plate velocities. Absolute velocities are low by approximately a factor of 10. This reflects the fact that the Rayleigh number for this case is a factor of 20 to 40 below that of the mantle. Since convective velocity scales approximately as the two-thirds power of the Rayleigh number, the absolute velocities are in reasonable agreement with observed values.

5. CONCLUSIONS

The sharp contrast in the character of the convective flow at high Rayleigh number between mostly internal heating and moderate heating from below provides a good basis for concluding that a substantial portion of the heating of the earth's mantle is from the core. This conclusion seems justified by the fact that dynamo action in the core to maintain the geomagnetic field against ohmic dissipation also appears to require a significant core heat flux. If this indeed is true, then these calculations indicate that the flow pattern in the mantle is dominated by a relatively small number of upwelling plumes. The pattern and spatial frequency character of the mid-ocean ridges would therefore be related to this system of localized upwelling flow.

These calculations imply that the computational tools are now available to perform relatively well-resolved three-dimensional simulations of the earth's interior. This capability, coupled with the recent advances in seismic techniques that provide three-dimensional observational data, suggests that significant new insights into the processes responsible for the earth's tectonic history may be imminent.

ACKNOWLEDGMENT

REFERENCES

1. G. Schubert, *Ann. Rev. Earth Planet. Sci.* 7:289 (1978).
2. A. M. Dziewonski, *J. Geophys. Res.* **89B7**:5929 (1984).
3. J. H. Woodhouse and A. M. Dziewonski, *J. Geophys. Res.* **89B7**:5953 (1984).
4. F. H. Busse and N. Riahi, *J. Fluid Mech.* **123**:283 (1982).
5. A. Zebib, G. Schubert, J. L. Dein, and R. C. Paliwal, *Geophys. Astrophys. Fluid Dyn.* **23**:1 (1983).
6. A. P. Boss, *Rev. Geophys. Space Phys.* **21**:1511 (1983).
7. J. R. Baumgardner, A three-dimensional finite element model for mantle convection, doctoral dissertation, UCLA (1983).
8. J. R. Baumgardner and P. O. Frederickson, *SIAM J. Num. Anal.*, in press.